Progress In Electromagnetics Research C, Vol. 78, 217–224, 2017

Ultra-Broadband Absorption with Gradient Pyramidal Metamaterials

Yuexia Liu, Wenliang Guo, and Tiancheng Han*

Abstract—We propose a novel absorber by integrating four different-sized pyramidal metamaterials into a unit cell, which leads to a super broadband absorption by properly selecting the geometrical parameters for each pyramid. It is found that in such a design strategy, the high-order modes may be excited and further enhanced by multi-layer overlapping between adjacent unit cells. The as-designed MA, which consists of 13 pairs of alternating metal-dielectric layers with a total thickness of 4.13 mm, shows an absorption of above 90% in the whole frequency range of 7–21.5 GHz. The full width at half maximum is 101.8%, and the ratio of operational bandwidth to thickness achieves 7. The proposed MA is 30% broader and 5.2% thinner than previously reported absorbers working in the same spectral region. Numerical result shows that the proposed absorber is independent of the polarization. The absorption decreases with fluctuations as the incident angle increases but remains quasi-constant up to relatively large angles. Such a design shows great promise for a broad range of applications at microwave frequencies, and the proposed scheme may be extended to the visible, infrared, terahertz spectral regions.

1. INTRODUCTION

For decades, perfect absorption has been central to various potential applications, such as sensors [1], micro-lens [2], energy harvesting [3–6], and radar stealth [7]. Compared to the traditional absorbers, such as quarter-wave antireflection coatings and surface relief structures that are limited by their large and bulk dimensions [8, 9], metamaterial absorbers (MAs) have attracted considerable attention from microwave to optical frequency by virtue of the perfect absorption, thin thickness and flexible design [10–13]. MAs are typically made of a patterned metal film above a homogeneous metal film with a dielectrics spacer [14–16]. Broadening the absorption bandwidth of MAs is very important for most practical applications such as stealth technology and energy harvesting. Broadband absorption has been presented by using saw-tooth anisotropic metamaterials [17, 18] or placing several different shaped resonators in one unit [19]. Beyond the optical frequency, many efforts have been made to broaden the absorption bandwidth of infrared absorbers [20–24] and THz absorbers [25–29]. For example, by combing two or four different resonators into one unit [20–22] and using double-layered structures [23, 24], the absorption bandwidth of infrared absorbers has been greatly expanded.

For applications of absorbers in the microwave frequency, the absorption bandwidth is one of the most important performance metrics. To achieve a broadband absorption in microwave frequency, a simple approach is to increase the loss of MA, such as loading lumped resistors [30, 31] and employing resistive ohmic sheets [32]. Another approach is to utilize multi-resonance by incorporating multiple resonators within one unit cell, which is limited by the number of resonators that can be used in practical situations [33]. Recently, by utilizing the concept of trapped rainbow effect [34], tapered hyperbolic metamaterials (THM) that consist of a metal-dielectric multilayer structure have been proposed to

Received 11 August 2017, Accepted 7 October 2017, Scheduled 17 October 2017
* Corresponding author: Tiancheng Han (tchan123@swu.edu.cn).
The authors are with the School of Physical Science and Technology, Southwest University, Chongqing 400715, China.

achieve broadband high absorption [35–37]. However, THM strategy generally has a disadvantage of large thickness due to the requirement of a number of layers. For example, an ultra-broadband absorber has been demonstrated by using two different-sized THM waveguides in one unit cell, which shows a strong absorption in most of the frequency range of 2.3–40 GHz when the thickness is 11.52 mm (48 pairs of alternating metal-dielectric layers) [35]. However, the absorption band above 0.9 is separated and relatively narrow.

In this paper, we construct an ultra-broadband MA by integrating four different-sized multilayered quadrangular frustum pyramids into a unit cell. These pyramids work at wide but different multiple absorbing bands, of which the overlapping leads to the super broadband absorption by properly selecting the geometrical parameters for each pyramid. The as-designed MA consists of 13 pairs of alternating metal-dielectric layers with a total thickness of 4.13 mm, which shows an absorption of above 90% in the whole frequency range of 7–21.5 GHz. The ratio of operational bandwidth to thickness ($W_{ob/t}$) achieves 7, which is much better than the single-sized pyramidal absorber (absorption above 90% from 7.8 to 14.7 GHz with a total thickness of 5 mm, $W_{ob/t} = 3.61$) [36] and the double-corrugated absorber (absorption above 90% from 7.8 to 16 GHz with a total thickness of 5 mm, $W_{ob/t} = 3.94$) [37]. More recently, broadening the bandwidth of the pyramidal absorber has been demonstrated by stimulating TM_{210} mode, which shows an absorption of above 90% from 7–18 GHz with a total thickness of 4.36 mm (composed of 20 pairs of alternating metal-dielectric layers) [38]. Quantitative comparison illustrates that our structure is 30% broader and 5.2% thinner than the absorber in [38].

2. MODELING AND SIMULATIONS

Electromagnetic wave impinging on an object can be transmitted, reflected or absorbed, which are related by the energy conservation law $T(\omega) + R(\omega) + A(\omega) = 1$, where $T(\omega)$, $R(\omega)$, and $A(\omega)$ are transmissivity, reflectivity, and absorptivity as functions of frequency ω, respectively. Generally, a homogeneous metal film is utilized as ground plane of the MAs, thus resulting in $T(\omega) = 0$ and $A(\omega) = 1 - R(\omega)$. High absorption $A(\omega)$ requires low reflectance $R(\omega)$ and efficient energy dissipation through excitation of the eigenmodes of the structure. By manipulating the magnetic resonance and electric resonance simultaneously, the effective impedance of MA will match the free space impedance once the MA satisfies the condition $\sqrt{\mu(\omega)/\varepsilon(\omega)} = Z_0$ [39]. As a result, the reflection is minimized, thus resulting in a perfect absorption of incident waves.

Figure 1(a) shows a unit cell of the proposed absorber that consists of four different-sized pyramids. One unit cell is divided into four equal portions, and each pyramid is located in the center of the corresponding portion. Each pyramid is composed of 13 pairs of alternating metal-dielectric layers with their sizes tapered linearly from top to bottom. The absorption frequency range is determined by the

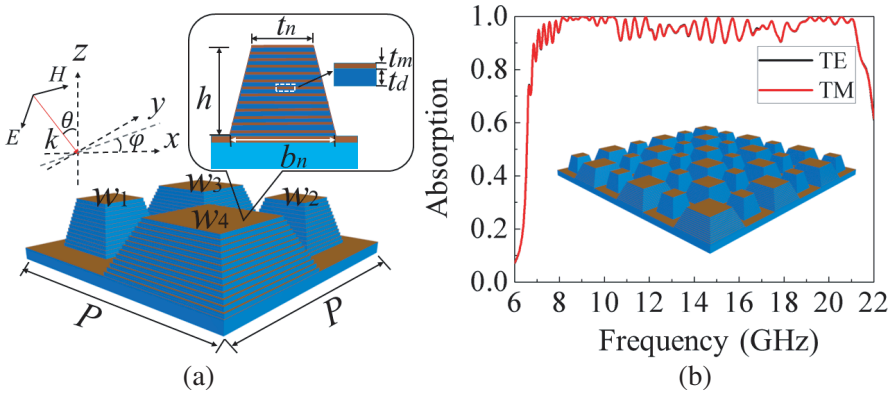

Figure 1. (Color Online) (a) Schematic of the proposed ultra-broadband MA made of four different-sized pyramids forming a square array of period P. The brown represents metal copper foils and the blue represents dielectric FR4. (b) The simulated absorption spectra of the as-designed MA under normally incident illumination.

top width and bottom width of each pyramid. In principle, a wide frequency range may be achieved by choosing a large difference between the top and bottom widths. However, there will emerge some low absorption bands between the high absorption bands if the number of metal-dielectric layers is not large enough [35]. Therefore, a balance has to be made between the total thickness of the structure and the absorption bandwidth, based on which the final goal is to achieve high efficient absorption with maximum bandwidth by employing the least number of metal-dielectric layers (corresponding to the thinnest thickness). We choose copper foils as the metal and lossy dielectric material epoxy-based FR4 as the dielectric spacer, which can be easily obtained and thus provides the benefit for large-area fabrication in practical applications. The copper foils have an electric conductivity of 5.0×10^7 S/m while the FR4 has a relative permittivity of $4.3(1 - 0.025i)$.

For each single pyramid w_i ($i = 1, 2, 3, 4$), it is found that the resonance frequency is mainly dominated by the patch size (t_n and b_n) and period P, and the absorbing efficiency is mainly dominated by the thickness of the dielectric spacer t_{d}. When the four pyramids are assembled into a period, a global optimization needs to be carried out. The goal of optimization is that the total absorption exceeds 90% with the bandwidth as wide as possible. The optimized dimensions of a unit cell shown in Fig. 1(a) are $P = 22.2\,\mathrm{mm}$, $t_{\mathrm{m}} = 0.018\,\mathrm{mm}$, $t_{\mathrm{d}} = 0.3\,\mathrm{mm}$, $b_1 = 6\,\mathrm{mm}$, $b_2 = 6.41\,\mathrm{mm}$, $b_3 = 9.1\,\mathrm{mm}$, $b_4 = 11\,\mathrm{mm}$, $t_1 = 3.96\,\mathrm{mm}$, $t_2 = 4.01\,\mathrm{mm}$, $t_3 = 6.16\,\mathrm{mm}$, $t_4 = 7.04\,\mathrm{mm}$, and the total thickness $h = 4.134\,\mathrm{mm}$. To examine the performance of the structure in Fig. 1(a), a full wave simulation is carried out based on the finite element method (FEM). In the simulation setup, periodic boundary conditions are used in the x and y directions, and the open boundary condition is used in the z-direction. A plane wave is incident downward on the MA with the electric field polarized along the x-direction (TE wave, transverse electric) and y-direction (TM wave, transverse magnetic). The simulated absorption spectra are demonstrated in Fig. 1(b). It is clear that the as-designed MA shows a strong absorption of above 0.9 in a wide frequency range $7 \sim 21.5\,\mathrm{GHz}$ for both TE and TM polarizations. The fluctuation in the absorption spectra indicates that the broadband absorption is attributed to the combination of many adjacent absorption peaks [36].

Relative absorption bandwidth (RAB) is usually adopted to evaluate the absorption performance of a MA, defined as $W_{\mathrm{RAB}} = 2(f_{\mathrm{U}} - f_{\mathrm{L}})/(f_{\mathrm{U}} + f_{\mathrm{L}})$, where f_{U} and f_{L} are the upper and lower limits of a frequency range with absorption $A(\omega)$ above 90%, respectively. The proposed MA in Fig. 1 possesses excellent absorption performance with $W_{\mathrm{RAB}} = 101.8\%$, which is much better than previously reported absorbers in Ref. [36] ($W_{\mathrm{RAB}} = 53.1\%$), Ref. [37] ($W_{\mathrm{RAB}} = 68.9\%$), and Ref. [38] ($W_{\mathrm{RAB}} = 88\%$). However, W_{RAB} cannot fully evaluate the overall performance of MAs since it does not take into account the thickness of MAs. Accordingly, a ratio of operational bandwidth to thickness can be used to evaluate the overall performance of a MA, defined as $W_{\mathrm{ob}/t} = 2(\lambda_{\mathrm{U}} - \lambda_{\mathrm{L}})/h$, where λ_{U} and λ_{L} are the upper and lower limits of a wavelength range with absorption $A(\omega)$ above 90%, respectively, and h is the thickness of the MA [38]. In our example, the MA exhibits a $W_{\mathrm{ob}/t}$ as large as 7, which is much better than previously reported absorbers working in the same spectral region, i.e., absorbers in Ref. [36] ($W_{\mathrm{ob}/t} = 3.61$), Ref. [37] ($W_{\mathrm{ob}/t} = 3.94$), and Ref. [38] ($W_{\mathrm{ob}/t} = 6.01$).

In addition to ultra-broadband property, it is also expected that the proposed MA is polarization independent for many practical applications. Fig. 2(a) presents the absorption spectra of the as-designed MA for different polarization angles from 0° (TM polarization) to 90° (TE polarization) under normally incident illumination. The polarization azimuthal angle is defined as the angle between the plane of incidence and the x axis of the coordinate. It is obvious that the absorption spectra are completely independent of the polarization angle of the incident wave. Beyond the case of normal incidence, it is necessary to examine whether the proposed MA is still insensitive to the polarization. Fig. 2(b) shows the influences of azimuthal angle on the absorption spectra at a fixed incident angle of 10°. Incident angle is defined as the angle between the incident wave vector and the z axis of the coordinate. It is seen that the absorption spectrum at the azimuthal angle of 45° is nearly the same as that of 0° and 90°. The results show that the proposed MA is very robust to the azimuthal angle.

Next we examine the performance of the as-designed MA under oblique incident illumination. Since the proposed MA is polarization independent, TM polarization ($\phi = 0°$) is taken as an example for the sake of convenience. Fig. 3(a) illustrates the absorption spectra of the proposed MA as a function of the incident angle. It is observed that the absorption spectra remain very high (above 90% in the whole frequency range of 7–21.5 GHz) up to a relatively large angle ($\theta = 20°$), and the absorption decreases

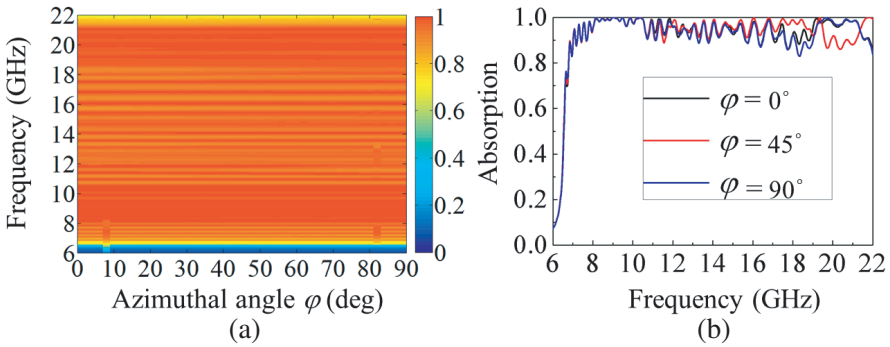

Figure 2. (Color Online) (a) Absorption map as a function of the azimuthal angle under normally incident illumination. (b) Absorption spectra for different azimuthal angles of $\phi = 0°$ (black), $\phi = 45°$ (red), and $\phi = 90°$ (blue) at a fixed incident angle of $\theta = 10°$.

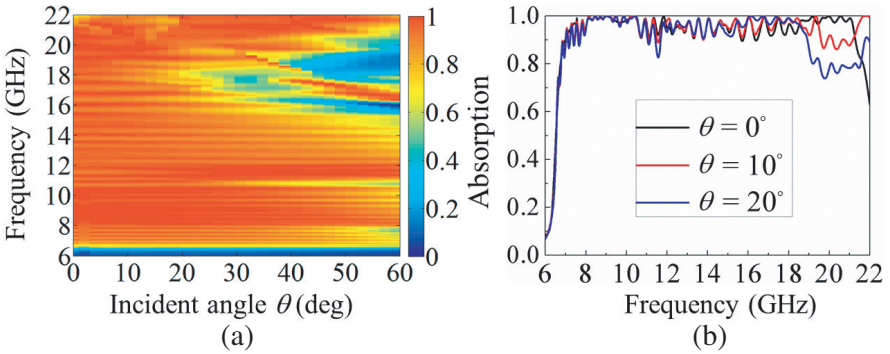

Figure 3. (Color Online) (a) Absorption map as a function of the incident angle at a fixed azimuthal angle $\phi = 0°$. (b) Absorption spectra for different incident angles of $\theta = 0°$ (black), $\theta = 10°$ (red), and $\theta = 20°$ (blue) at a fixed azimuthal angle of $\phi = 45°$.

with fluctuations as the incident angle increases. This is because the magnetic component of the incident wave drops rapidly as the angle increases, which strongly deteriorates the magnetic resonances. The influences of incident angle on the absorption spectra are also investigated at a fixed azimuthal angle of 45°, as shown in Fig. 3(b).

3. DISCUSSION

To understand the mechanism of the proposed MA, we investigate the single-pyramidal MA that is formed by removing the other three pyramids of Fig. 1(a). Fig. 4(a) presents the absorption spectra of the four single-pyramidal MAs, denoted as w_4, w_3, w_2, and w_1, respectively. Obviously, there are four distinct absorption bands with absorptivity above 80%, i.e., 6.5–10 GHz, 8–12 GHz, 11.8–18.2 GHz, and 12–18.5 GHz. These discrete absorption bands can be interpreted by the standing wave resonance mechanism [15]. The metal-dielectric-metal structure can be considered as a waveguide, in which the standing wave resonances are generated when the EM waves from adjacent gaps propagate oppositely in the spacer layer. The absorption peaks of the metamaterial absorber result from the standing wave dissipated in the lossy dielectric spacer layer. The resonance frequency of the standing wave can be described as

$$f_{sw} = m\frac{c}{2\sqrt{\varepsilon_r}L} \tag{1}$$

where L, c, m, and ε_r are the length of the dielectric slit, the speed of light in vacuum, the mode number of the harmonic, and the relative permittivity, respectively. After substituting the related parameters of the MAs to the above equation, the fundamental harmonic frequency bands of w_4, w_3, w_2, and w_1

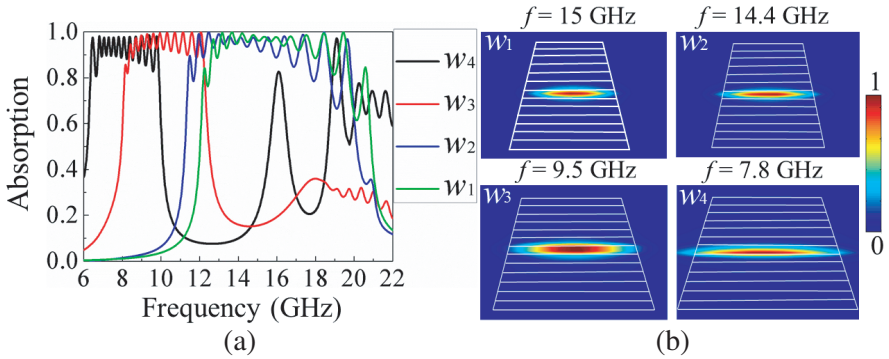

Figure 4. (Color Online) (a) Absorption spectra of the four single-pyramidal MAs that are formed by removing the other three pyramids of Fig. 1(a). (b) Magnetic field distributions for different pyramids at the resonance frequency of 15 GHz, 14.4 GHz, 9.5 GHz, and 7.8 GHz, respectively.

can be calculated to be 6.5–10.3 GHz, 8–11.7 GHz, 11.3–18 GHz, and 12.1–18.3 GHz, respectively, which agree very well with the simulation results. Obviously, the first order standing wave harmonic leads to the strong absorption peak. By simply merging absorption peaks of the unit cells in each layer, a continuous broadband absorption is achieved [35, 36].

Without loss of generality, we take the 7th layer of each pyramid as an example to approve the aforementioned broadband absorption mechanism of the proposed MAs. Fig. 4(b) shows the magnetic field distributions for different pyramids at different resonance frequencies, i.e., f = 15, 14.4, 9.5, and 7.8 GHz. We can obtain the theoretical values f_{sw} = 14.8, 14.1, 9.6, and 7.9 GHz, respectively, which agree well with the simulation results. Obviously, each resonance is localized in a specific pyramid, where a smaller pyramid corresponds to a higher resonance frequency.

We then pay attention to the strong absorption band at 18.5–21.5 GHz, which is mainly attributed to the high-order modes of the two big pyramids, i.e., w_3 and w_4. We simulate the magnetic field distributions of the proposed MA at two specific resonance frequencies, i.e., f = 18.8 and 21.2 GHz. From Fig. 5 we can see that only fundamental harmonics are supported in the two small pyramids (w_1 and w_2), while the high-order modes appear in the two big pyramids (w_3 and w_4). With the increase of frequency, the fundamental harmonics become weaker and weaker, and the main contribution of perfect absorption comes from high-order modes. Inspired by the pioneering work [38], the resonance frequencies (f_{mnl}) of high-order modes for the rectangular waveguide cavity resonators can be expressed as

$$f_{sw} = \frac{c}{2\sqrt{\varepsilon_r}}\sqrt{\frac{m^2}{L^2} + \frac{n^2}{L^2} + \frac{l^2}{d^2}} \tag{2}$$

where L and d are the resonator sizes. The indices m, n, l represent the variation number in the

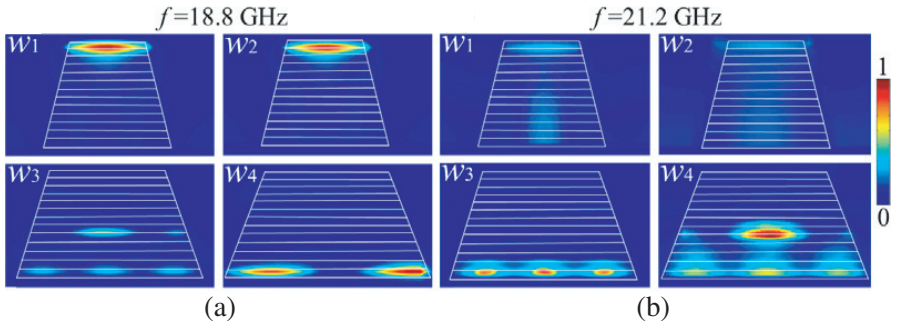

Figure 5. (Color Online) (a) Magnetic field distribution of the proposed MA at the resonance frequency of 18.8 GHz. (b) Magnetic field distribution of the proposed MA at the resonance frequency of 21.2 GHz.

standing wave patterns along the x, y, z directions, respectively. Equation (2) describes all the possible resonant modes along three directions. In our scheme, the high-order modes frequency bands of w_3 and w_4 can be calculated to be 17.7–22 GHz and 14.5–22 GHz, respectively. Quantitative comparison with Fig. 4(a) finds that the calculated results agree well with the simulated ones. To conclude, the broad absorption bandwidth comes from two sources: the fundamental harmonics of the four pyramids and the high-order modes of the two big pyramids.

4. CONCLUSION

In summary, by employing both fundamental harmonics and high-order modes, an ultra-broadband and high-efficiency absorber has been designed through integrating four different-sized pyramidal metamaterials into a unit cell. The as-designed MA shows an absorption of above 90% in the whole frequency range of 7–21.5 GHz, which demonstrates much better performance than the previously reported absorbers working in the same spectral region. The ultra-broadband property makes it a good candidate for the design of a high-performance absorber with the applications targeted in stealth, camouflage, and antenna at microwave frequencies. More importantly, such a scheme is believed to be capable of extending to the visible, infrared, and THz spectral regions.

ACKNOWLEDGMENT

This work was supported by the National Natural Science Foundation of China (NSFC) (11304253), the Research Fund for the Doctoral Program of Higher Education of China (20130182120024), and the Fundamental Research Funds for the Central Universities (XDJK2016A019).

REFERENCES

1. Li, W. and J. Valentine, "Metamaterial perfect absorber based hot electron photodetection," *Nano Lett.*, Vol. 14, 3510–3514, 2014.
2. Song, Y. M., Y. Xie, V. Malyarchuk, J. L. Xiao, I. Jung, K. J. Choi, Z. Liu, H. Park, C. Lu, R. H. Kim, and R. Li, "Digital cameras with designs inspired by the arthropod eye," *Nature*, Vol. 497, 95–99, 2013.
3. Yin, X., L. Chen, and X. Li, "Ultra-broadband super light absorber based on multi-sized tapered hyperbolic metamaterial waveguide arrays," *J. Lightwave Technol.*, Vol. 33, 3704–3710, 2015.
4. Xiao, S., T. Wang, Y. Liu, C. Xu, and X. Yan, "Tunable light trapping and absorption enhancement with graphene ring arrays," *Phys. Chem. Chem. Phys.*, Vol. 18, 26661–26669, 2016.
5. El-Toukhy, Y. M., M. Hussein, M. F. O. Hameed, and S. S. A. Obayya, "Characterization of asymmetric tapered dipole nanoantenna for energy harvesting applications," *Plasmonics*, Vol. 12, 1–8, 2017.
6. El-Toukhy, Y. M., M. F. O. Hameed, M. Hussein, and S. S. A. Obayya, "Tapered plasmonic nanoantennas for energy harvesting applications," *Nanoplasmonics — Fundamentals and Applications*, 2017, DOI: 10.5772/67418.
7. Ni, X., Z. J. Wong, M. Mrejen, Y. Wang, and X. Zhang, "An ultrathin invisibility skin cloak for visible light," *Science*, Vol. 349, 1310–1314, 2015.
8. Chen, Y., P. Han, and X.-C. Zhang, "Tunable broadband antireflection structures for silicon at terahertz frequency," *Appl. Phys. Lett.*, Vol. 94, 041106, 2009.
9. Kim, D.-H., D.-S. Kim, S. Hwang, and J.-H. Jang, "Surface relief structures for a flexible broadband terahertz absorber," *Opt. Express*, Vol. 20, 16815–16822, 2012.
10. Landy, N. I., S. Sajuyigbe, J. J. Mock, D. R. Smith, and W. J. Padilla, "Perfect metamaterial absorber," *Phys. Rev. Lett.*, Vol. 100, 207402, 2008.
11. Watts, C. M., X. L. Liu, and W. J. Padilla, "Metamaterial electromagnetic wave absorbers," *Adv. Mater.*, Vol. 24, OP98–OP120, 2012.

12. El-Aasser, M. A., "Design optimization of nanostrip metamaterial perfect absorbers," *J. Nanophotonics*, Vol. 8, 11, 2014.
13. Hedayati, M. K., M. Javaherirahim, B. Mozooni, R. Abdelaziz, A. Tavassolizadeh, V. S. K. Chakravadhanula, V. Zaporojtchenko, T. Strunkus, F. Faupel, and M. Elbahri, "Design of a perfect black absorber at visible frequencies using plasmonic metamaterials," *Adv. Mater.*, Vol. 23, 5410, 2011.
14. Hao, J., J. Wang, X. Liu, W. J. Padilla, L. Zhou, and M. Qiu, "High performance optical absorber based on a plasmonic metamaterial," *Appl. Phys. Lett.*, Vol. 96, 251104, 2010.
15. Peng, X., B. Wang, S. Lai, D. Zhang, and J. Teng, "Ultrathin multi-band planar metamaterial absorber based on standing wave resonances," *Opt. Express*, Vol. 20, 27756–27765, 2012.
16. Grant, J., Y. Ma, S. Saha, L. B. Lok, A. Khalid, and D. R. S. Cumming, "Polarization insensitive terahertz metamaterial absorber," *Opt. Lett.*, Vol. 36, 1524–1526, 2011.
17. Zhu, P. and L. J. Guo, "High performance broadband absorber in the visible band by engineered dispersion and geometry of a metal-dielectric-metal stack," *Appl. Phys. Lett.*, Vol. 101, 241116, 2012.
18. Cui, Y., K. H. Fung, J. Xu, H. Ma, Y. Jin, S. He, and N. X. Fang, "Ultrabroadband light absorption by a sawtooth anisotropic metamaterial slab," *Nano Lett.*, Vol. 12, 1443–1447, 2012.
19. Azad, A. K., W. J. Kortkamp, M. Sykora, N. R. Weissebernstein, T. S. Luk, and A. J. Taylor, "Metasurface broadband solar absorber," *Sci. Rep.*, Vol. 6, 20347, 2016.
20. Koechlin, C., P. Bouchon, F. Pardo, J. Jaeck, X. Lafosse, J.-L. Pelouard, and R. Haidar, "Total routing and absorption of photons in dual color plasmonic antennas," *Appl. Phys. Lett.*, Vol. 99, 241104, 2011.
21. Cui, Y., J. Xu, K. H. Fung, Y. Jin, A. Kumar, S. He, and N. X. Fang, "A thin film broadband absorber based on multi-sized nanoantennas," *Appl. Phys. Lett.*, Vol. 99, 253101, 2011.
22. Bouchon, P., C. Koechlin, F. Pardo, R. Haïdar, and J. L. Pelouard, "Wideband omnidirectional infrared absorber with a patchwork of plasmonic nanoantennas," *Opt. Lett.*, Vol. 37, 1038–1040, 2012.
23. Feng, R., J. Qiu, L. Liu, W. Ding, and L. Chen, "Parallel *LC* circuit model for multi-band absorption and preliminary design of radiative cooling," *Opt. Express*, Vol. 22, A1713–A1724, 2014.
24. Guo, W., Y. Liu, and T. Han, "Ultra-broadband infrared metasurface absorber," *Opt. Express*, Vol. 24, 20586–20592, 2016.
25. Ye, Y. Q., Y. Jin, and S. L. He, "Omnidirectional, polarization-insensitive and broadband thin absorber in the terahertz regime," *JOSA B*, Vol. 27, 498–504, 2010.
26. Amin, M., M. Farhat, and H. Bagci, "An ultra-broadband multilayered graphene absorber," *Opt. Express*, Vol. 21, 29938–29948, 2013.
27. Zhu, J., Z. Ma, W. Sun, F. Ding, Q. He, L. Zhou, and Y. Ma, "Ultra-broadband terahertz metamaterial absorber," *Appl. Phys. Lett.*, Vol. 105, 021102, 2014.
28. Liu, S., H. Chen, and T. J. Cui, "A broadband terahertz absorber using multi-layer stacked bars," *Appl. Phys. Lett.*, Vol. 106, 151601, 2015.
29. Peng, Y., X. Zang, Y. Zhu, C. Shi, L. Chen, B. Cai, and S. Zhuang, "Ultra-broadband terahertz perfect absorber by exciting multi-order diffractions in a bouble-layered grating structure," *Opt. Express*, Vol. 23, 2032–2039, 2015.
30. Li, S., J. Gao, X. Cao, W. Li, Z. Zhang, and D. Zhang, "Wideband, thin and polarization-insensitive perfect absorber based the double octagonal rings metamaterials and lumped resistances," *J. Appl. Phys.*, Vol. 116, 043710, 2014.
31. Yang, J. and Z. X. Shen, "A thin and broadband absorber using double-square loops," *IEEE Antennas Wireless Propag. Lett.*, Vol. 6, 388–391, 2007.
32. Li, M., S. Xiao, Y. Y. Bai, and B. Z. Wang, "An ultrathin and broadband radar absorber using resistive FSS," *IEEE Antennas Wireless Propag. Lett.*, Vol. 11, 748–751, 2012.
33. Yoo, Y. J., Y. J. Kim, P. V. Tuong, J. Y. Rhee, K. W. Kim, W. H. Jang, Y. H. Kim, H. Cheong, and Y. Lee, "Polarization-independent dual-band perfect absorber utilizing multiple magnetic

resonances," *Opt. Express*, Vol. 21, 32484–32490, 2013.

34. Jiang, T., J. Zhao, and Y. Feng, "Stopping light by an air waveguide with anisotropic metamaterial cladding," *Opt. Express*, Vol. 17, 170–177, 2009.
35. Yin, X., C. Long, J. Li, H. Zhu, L. Chen, J. Guan, and X. Li, "Ultra-wideband microwave absorber by connecting multiple absorption bands of two different-sized hyperbolic metamaterial waveguide arrays," *Sci. Rep.*, Vol. 5, 15367, 2015.
36. Ding, F., Y. Cui, X. Ge, Y. Jin, and S. He, "Ultra-broadband microwave metamaterial absorber," *Appl. Phys. Lett.*, Vol. 100, 103506, 2012.
37. Pang, Y., H. Cheng, Y. Zhou, and J. Wang, "Double-corrugated metamaterial surfaces for broadband microwave absorption," *J. Appl. Phys.*, Vol. 113, 084907, 2013.
38. Long, C., S. Yin, W. Wang, W. Li, J. Zhu, and J. Guan, "Broadening the absorption bandwidth of metamaterial absorbers by transverse magnetic harmonics of 210 mode," *Sci. Rep.*, Vol. 6, 21431, 2016.
39. Tassin, P., T. Koschny, M. Kafesaki, and C. M. Soukoulis, "A comparison of graphene, superconductors and metals as conductors for metamaterials and plasmonics," *Nature Photon.*, Vol. 6, 259–264, 2012.